Enhanced Nitrogen Photofixation over $LaFeO_3$ via Acid Treatment

Xiang Sun,[†,‡,§] Dong Jiang,[†,§] Ling Zhang,[†] Songmei Sun,[†] and Wenzhong Wang*[,†]

[†]State Key Laboratory of High Performance Ceramics and Superfine Microstructure, Shanghai Institute of Ceramics, Chinese Academy of Sciences, 1295 Dingxi Road, Shanghai 200050, P. R. China

[‡]University of Chinese Academy of Sciences, Beijing 100049, P. R. China

* Supporting Information

ABSTRACT: The N_2 photofixation presents a green and eco-friendly ammonia synthesis approach. However, present strategies for light-induced N_2 activation suffer from low efficiency and instability, largely hindering the development of this technology. Herein, we report the $LaFeO_3$ co-optimization of N_2 activation as well as subsequent photoinduced protonation with the further phosphate acid treatment. Efficient ammonia evolution rate reached 250 μmol g^{-1} h^{-1} over $LaFeO_3$ under simulated sunlight with appropriate acid treatment. The enhancement of phosphate modified samples was mainly attributed to the "pull and push" effect. The hydrogen bonding centers and transition metals (Fe) served as two separation active sites, which improves the adsorption and activation of dinitrogen. In addition, the facilitation of H_2O dissociation was also achieved after phosphate modification. These results suggested an alternative N_2 photofixation strategy of traditional organic and precious metallic additives for efficient ammonia synthesis.

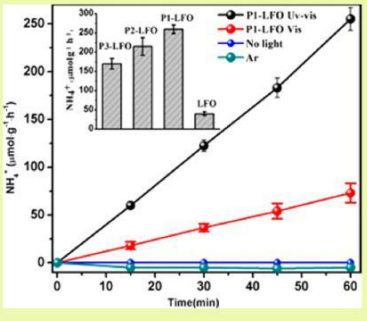

KEYWORDS: N_2 photofixation, surface modification, proton, photocatalysis, hydrazine

INTRODUCTION

Nitrogen (N_2) fixation to ammonia (NH_3) is the second most important chemical process in nature next to photosynthesis.[1−3] Artificial N_2 fixation is of growing importance in various modern industrial and agricultural fields with the development of human society. The industrial Haber−Bosch method process is generally conducted under severe conditions (300−550 °C, 150−250 MPa) because of the stubborn triple bond of N_2 toward dissociation (944 kJ mol^{-1}), consuming 1−2% of world electricity and generating 300 million tons of carbon dioxide as side product per year.[4−6] Catalysts that were applied to energy-efficient N_2 fixation have been studied for 100 years, despite the recent progress in solar-driven N_2 reduction by water with semiconductors at mild reaction conditions. The involved photocatalysts still suffer from low efficiency even in the presence of various hole-scavengers or cocatalysts. With consideration of the global energy crisis as well as climate change, efficient ammonia synthesis under mild conditions is still a scientific challenge remaining to be met.

The effective activation of N N triple bonds and the subsequent protonation process of dinitrogen are considered to be the bottlenecks of N_2 photofixation. Recently, construction of surface defects on the photocatalysts including Bi-based photocatalysts, g-C_3N_4, or TiO_2 has been regarded as a popular strategy.[7−9] In contrast, for the biogeochemical N_2 cycle, a molybdenum−iron (MoFe) containing protein within the nitrogenase activates N_2 molecules using the core MoFe cofactor which cleaves the stable N_2 under mild conditions through the "pull and push" hypothesis. The "push−pull" hypothesis of N_2 activation is the synergetic effect of metal and Lewis acid centers, in which electron density is "pushed" from a reduced transition metal center and "pulled" into the N_2 unit by adjacent hydrogen bonding sites.[10] The "push" effect is that the transitional metals (metal = Fe, Mo, Ni, Co, etc.) donate their available d-orbital electrons to π N N antibonding to activate the N_2 ligand.[11] For instance, the Fe^{3+} ions insert at the interstitial position of g-C N and are stabilized in g-C N through the coordinative Fe N bonding, which was proven to be the active sites for the adsorption and activation of N_2.[12] The Fe^{3+} ions doped in the semiconductors are easy to reduce to Fe^{2+} by photogenerated electrons, which also promotes the activation of N_2.[13] Chang et al. also reported that the Cr^{3+} ions in Cr-MIL101 played the vital role in thermodynamically capturing nitrogen over methane and oxygen with a large N_2 uptake. According to these results, the unsaturated transition metal sites show the capability to strongly adsorb the N due to the available electrons donated into the N N antibonding. The "pull" effect is from the acidic sites (including hydrogen bonding) in the secondary sphere of the nitrogenase, which plays a crucial role in facilitating N_2 activation with low overpotential and high selectivity.[15,16] The dinitrogen molecule with lone pair electrons presents the character of Lewis base, and is thus more easily chemisorbed on the surface with Lewis acid character.[17] Hydrogen bonding groups (from such as phosphate or hydrofluoric) and Lewis acidic sites are used in metallic enzymes to modulate substrate binding and activation. The two effects may synergistically contribute to the low overpotential and high protonation selectivity in the enzyme;

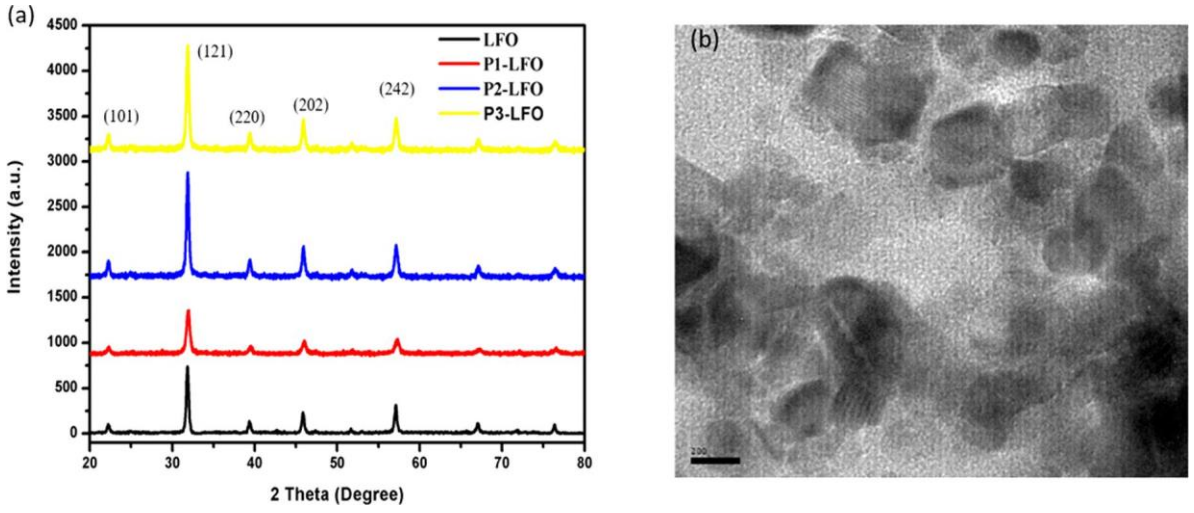

Figure 1. (a) XRD patterns of $LaFeO_3$ and P-LFO series samples. (b) The TEM image of phosphate modified sample of P1-LFO.

thus, the N N triple bonds are hydrogenated gradually via the successive transfer of electrons and protons which lower the high activation energy of N_2.[18] According to the examples of enzymatic catalysts, the efficient approach for N_2 activation and hydrogenation relies on the concomitant transfer of protons and electrons, which stem from acids and reduction equivalents, respectively.[19]

As the imitation of biogeochemistry, the solar-driven N_2 reduction is also performed under moderate reaction conditions accompanied by the photogenerated electrons and H_2O-derived proton transfer, while its efficiency is still low because of the recombination of the photogenerated carriers, inefficient withdrawing of proton from water, and the hydrogenation process of activated N_2. Inspired by the "pull and push strategy", we chose the transition metal dominated perovskite structure $LaFeO_3$ (LFO) as the photocatalyst. With the consideration of the relatively low N_2 photofixation ability of sole $LaFeO_3$, phosphate groups were modified on the surface of $LaFeO_3$ to mimic the electron transfer between the ATP and the FeMo factor, which play the critical role in the activation of the N_2 triple bond and facilitates the hydrogenation process of N_2. Furthermore, the phosphates (phospholipids) are known to play vital roles in both transferring electrons in electron-transport chains and pumping protons to drive chemical synthesis during the light-dependent reactions including the H_2 production and CO_2 fixation.[20] In this way, phosphate-involving photofixation was mimicked to improve the N_2 photofixation ability of $LaFeO_3$. The perovskite $LaFeO_3$ surface modified with phosphate acid exhibited efficient photocatalytic activity for ammonia synthesis (250 μmol g^{-1} h^{-1}) under simulated sunlight.

EXPERIMENTAL SECTION

Synthesis of the Samples. All the reagents were of analytic purity and used as received from Sinopharm Reagent Co. Ltd. $LaFeO_3$ photocatalyst was synthesized via a hydrothermal method. Briefly, 2 mmol of $La(NO_3)_3$ and 2 mmol of $Fe(NO_3)_3{\cdot}9H_2O$ were dissolved in 40 mL of deionized water. An 8 mmol portion of citric acid was added into the above solution under continuous stirring. Afterward, the solution was transferred into a 50 mL Teflon-lined stainless steel autoclave and kept at 160 °C for 10 h. After the reaction mixture cooled to room temperature, the obtained precipitate was rinsed by deionized water several times and then dried at 60 °C overnight, followed by calcination at 750 °C for 3 h. Phosphate modified $LaFeO_3$ (P-LFO, samples are noted as Pn-LFO, n = 1, 2, 3, n indicates the phosphate concentration) was obtained by immersing $LaFeO_3$ powders in the H_3PO_4 solution with an initial concentration of 0.1, 0.2, and 0.3 mmol/L, respectively, followed by calcination at 500 °C for 2 h.

Chemicals and Characterization. The purity and crystallinity were characterized by powder X-ray diffraction (XRD) with a Rigaku D/MAX 2250 V diffractometer using monochromateted Cu Kα (λ = 0.15418 nm) radiation. Diffuse reflectance spectra were obtained on a UV−vis spectrophotometer (Hitachi U-3010) using $BaSO_4$ as the reference. The morphology and microstructure of samples were examined by TEM using a TecnaiG2 F20 S-Twin. The N_2 temperature-programmed desorption (N_2-TPD) analysis was performed on a Micromeritics ChemiSorb 2750, equipped with a thermal conductivity detector. For each sample (30 mg), after pretreatment with a He flow at 400 °C for 2 h in a quartz tube, the N_2 adsorption was performed in a N_2 gas flow at the rate of 30 mL/min at room temperature. Afterward, the sample was heated to 500 °C at a heating rate of 10 °C/min under high pure He gas flow. The hydroxyl radicals produced on the surface of $LaFeO_3$ were examined in 100 mL of deionized water with 50 mg of photocatalyst under the Xe lamp. X-ray photoelectron spectroscopy (XPS) analysis was performed on an ESCALAB 250 instrument (Thermo Scientific Ltd.). The C 1s signal was used to calibrate the charge effects. Infrared (IR) spectra were recorded on KBr/$LaFeO_3$ pellets (1 wt % $LaFeO_3$ or P-LFO) in a Burker Tensor 27 spectrometer. After accumulation of 64 scans, the spectra were collected with a resolution of 4 cm^{-1}. BET surface area was performed on a Micromeritics ASAP 2000 analyzer. In situ diffuse reflectance FTIR spectra were also recorded by a Bruker Tensor 27 spectrometer, with a designed reaction cell. Then, the high purity Ar was used to pump out all the gases in the reaction cell and was adsorbed on the photocatalyst surface. Afterward, the N_2 was pumped in to construct the nitrogen atmosphere over the P1-LFO sample. The photoluminescence (PL) spectrum was measured with a Hitachi F-4600 spectrophotometer at room temperature (excitation wavelength = 360 nm).

Nitrogen Photofixation. N_2 photofixation was carried out in a homemade gas−solid reaction system. Briefly, 0.02 g of phosphate modified $LaFeO_3$ was uniformly dispersed on the alumina sample platform in a glass reactor (600 mL), and 40 mL of water was injected into the reactor as the proton source. High purity N_2 was flowed into the reaction system with a different velocity ratio. Then, the reaction system was exposed to the full-spectrum irradiation of a 500 W Xe lamp. The visible light was obtained with a λ > 420 nm high pass filter. The products were expelled outside the reactor by continuous flow and finally trapped in 160 mL of 0.05 M H_2SO_4 absorption liquid. Prior to any light irradiation, N_2 was kept flowing into the reactor for 1 h to exclude the O_2 thoroughly. After the reaction, the remained H_2O

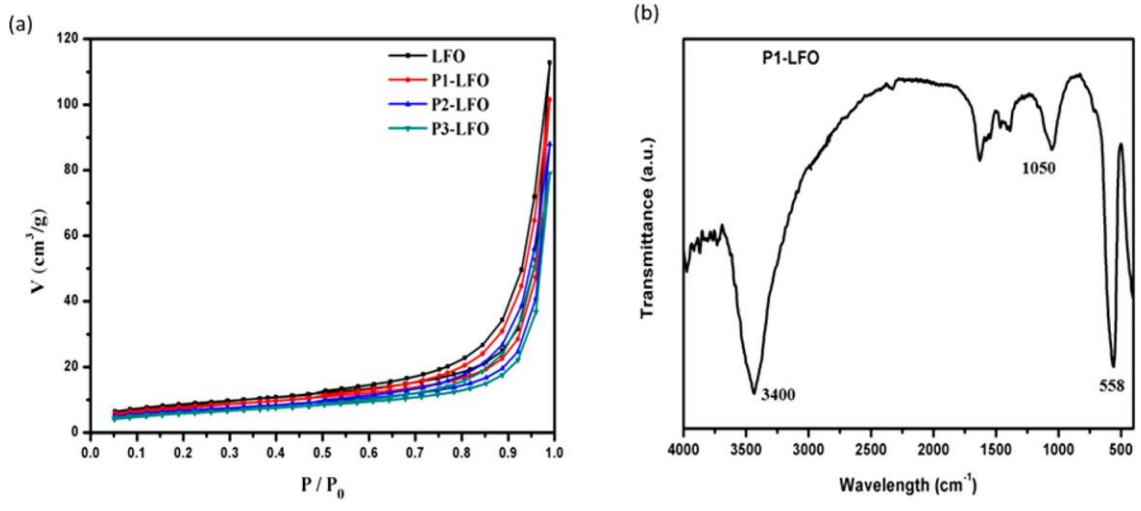

Figure 2. (a) N_2 adsorption−desorption isotherms of the products. (b) FTIR spectrum of P1-LFO with the characteristic absorption band of phosphate.

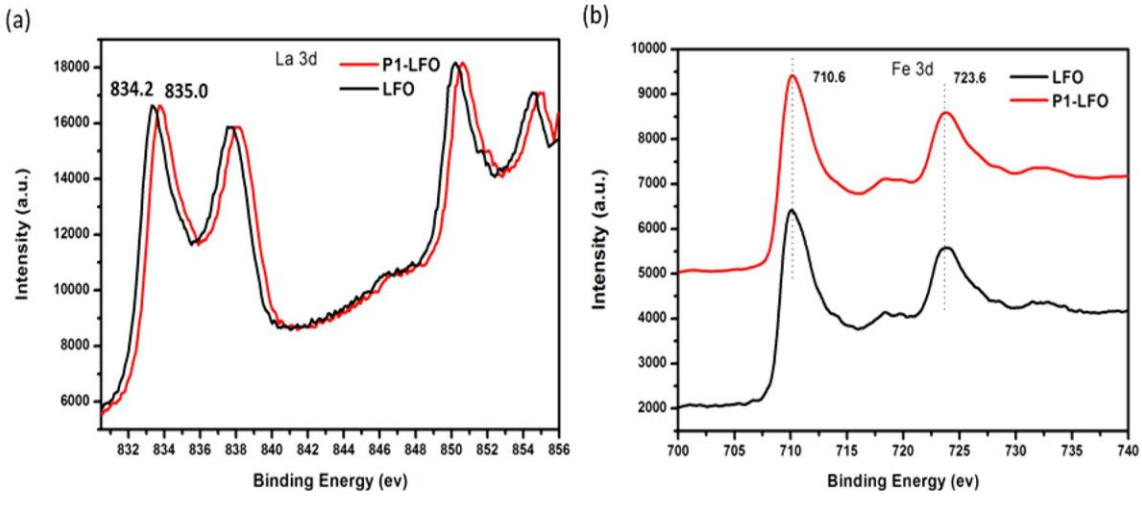

Figure 3. XPS spectrum of (a) La 3d and (b) Fe 3d in LFO and P1-LFO, respectively.

in the reactor was also transformed into the absorption liquid to avoid the loss of any products. The concentration of ammonia was measured using Nessler's reagent spectrophotometry method. The N_2H_4 formed during the reaction was measured via using the 4-dimethylamino-benzaldehyde spectrophotometry method.

Computational Methods. All of the calculations were performed using the CASTEP package in the Accelrys Material studio modeling suite using periodic DFT. The Perdew−Burke−Ernzerhof (PBE) exchange-correlation functional was used within the spin-polarized generalized gradient approximation (GGA). The (121) facets of polycrystal $LaFeO_3$ were chosen to perform DFT simulations. A (3 × 3) supercell with the vacuum thickness of 15 Å was modeled. In order to get exact results, the electronic state was expanded using plane waves as a basis set as with a cut of 420 eV, and the Brillouin zone was sampled using a 2 × 3 × 1 Monkhorst−Pack k-grid.

Photoelectrochemical Analysis. The photoelectrochemical measurements were performed on a CHI 660D electrochemical workstation (Shanghai Chenhua, China) using a standard three-electrode cell in which 0.5 M Na_2SO_4 solution was used as electrolyte, with a working electrode, a platinum wire as counter electrode, and a saturation mercury electrode (RHE) as the reference electrode. To make a working electrode, 20 mg of catalyst was suspended in 0.5 mL of ethanol, and the mixtures were ultrasonically scattered for 5 min to form a homogeneous mixture. Then, 0.1 mL of slurry was dropped on the fluorine doped tin oxide (FTO) glass (1.5 cm × 2 cm). After evaporation of ethanol in the air, the electrode was calcined at 300 °C for 2 h. Before the photocurrent measurement, N_2 or Ar gas was purged into the Na_2SO_4 aqueous solution to remove the dissolved molecular oxygen for 30 min and kept purging during the photocurrent measurement. Electrochemical impedance spectroscopy (EIS) measurements were employed to study the transportation and separation of photogenerated charge carriers. A 0.5 M of Na_2SO_4 electrolyte containing 5 mmol of Fe $(CN)_6^{3-/4-}$ was applied. The influence on the proton transfer after phosphate modification was investigated by linear sweep voltammetry (LSV). LSV was conducted over the potential range −0.6 to 0.1 V with a scan rate of 1 mV/s.

RESULTS AND DISCUSSION

Characterization. As indicated in Figure 1a, the surface phosphate modifications did not change the orthorhombic perovskite structure of $LaFeO_3$. The XRD pattern of the $LaFeO_3$ shows the sharp diffraction peaks at 22.6°, 33.2°, 39.7°, 46.2° and 57.4°, which can be indexed to the planes (101), (121), (220), (202) and (242) of $LaFeO_3$ (JCPDS 37-1493).[21] The detailed characterization of the morphologies of the photocatalyst is based on the TEM. It is clear that the phosphate modified $LaFeO_3$ (P1-LFO) exhibits the nanoplate morphology with the size between 200 and 350 nm (shown in Figure 1b).

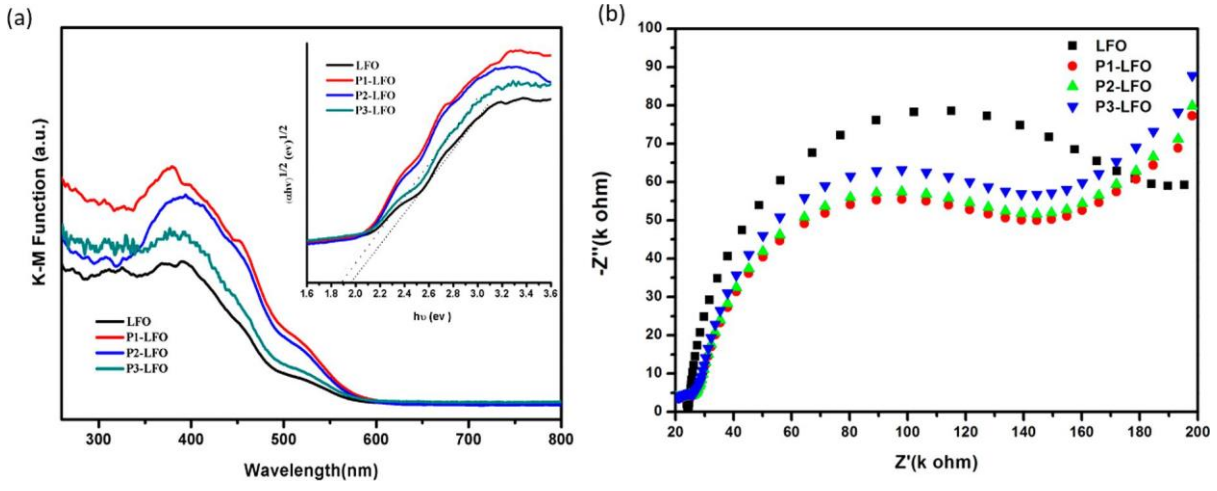

Figure 4. (a) UV−vis absorption spectra of LFO and P-LFO. Inset shows plots of $(\alpha h\nu)^{1/2}$ versus photon energy (hν) of LFO and P-LFO. (b) EIS Nyquist plots with Xe lamp irradiation over LFO and P-LFO series samples.

The BETs of the surface area of the pristine $LaFeO_3$ and P-LFO series samples have been measured. As can be seen from Figure 2a, the pristine $LaFeO_3$ exhibits the specific surface area of 15 m^2/g while the P-LFO series samples show a slight small value in the range 12.4−14.5 m^2/g. The phosphate modification has little influence on the BET surface area of the composites, implying that the negligible effect from surface area on the followed N_2 photofixation performance. The successful modification of phosphate was confirmed by FTIR as well as XPS. As shown in Figure S1, the absorption peak at the 3400 cm^{-1} is assigned to be the OH bending mode of the adsorbed water and the OH group. The band at 1644 cm^{-1} corresponds to the asymmetric stretching of the carboxyl root. The less intense band at 1387 and 1025 cm^{-1} corresponds to the principle vibration of the carbonate CO_3^{2-} group and ν_3 asymmetric stretching of metal carbonates, which were not detected by the XRD.[22] In addition, two sharp peaks at 558 and 420 cm^{-1}, which are attributed to the Fe−O stretching mode and the O−Fe−O bending mode, respectively. Compared with pristine $LaFeO_3$, the enhanced absorption peak at 3400 cm^{-1} of the P1-LFO sample is assigned to the adsorbed water or OH groups from phosphate groups, indicating the formation of hydrogen bonding after phosphate modification. The strong absorption at 1050 cm^{-1} (shown in Figure 2b) indicates the presence of PO_4^{3-} groups on the $LaFeO_3$ surface.[23]

X-ray photoelectron spectroscopy (XPS) was used to investigate the surface chemical environment of both $LaFeO_3$ and P1-LFO samples. As further proof for the modification, the P 2p peak (shown in Figure S2) for $LaFeO_3$ is centered at 133.6 eV, which is assigned to be the characteristic of the pentavalent oxidation state (P^{5+}) in the form of the P−O bond. As shown in Figure 3a, the La $3d_{5/2}$ peak of the pristine $LaFeO_3$ centered at ca. 834.2 eV shows the typical complex structure of core-level photoemission spectra of the light rare earth compounds. In addition, the well-known spin−orbit multiplet splitting, a characteristic satellite structure of La 3d, is present, which has been mainly attributed to final-state effects or to charge-transfer coexcitations.[24] After phosphate modification, the La 3d spectrum of P1-LFO exhibits a positive shift of 0.6 eV compared with that of pristine $LaFeO_3$, indicating the binding between La^{3+} and phosphate with the formation of La-PO_3^- species. In contrast, the Fe 3d spectrum of both P1-LFO and LFO remained unchanged, implying almost no interaction between the phosphate and Fe^{3+} (Figure 3b). It is mainly because La^{3+} shows a superior basicity than that of Fe^{3+} that results in the preferential combination with phosphate. It can be first concluded that two different and separation active sites are formed, transition metal Fe^{3+} and phosphate species. The O 1s signals of P1-LFO (shown in Figure S3) show two peaks at 530.1 and 532.9 eV. The main peak at 530.1 eV could be ascribed to the contribution of La−O and Fe−O in the $LaFeO_3$ crystal lattice. The O_H XPS is closely related to the hydroxyl groups resulting mainly from the chemisorbed water or surface hydroxyl groups from PO_4^{3-}.[25] Compared with P1-LFO, the O 1s signal of LFO just exhibited the presence of lattice oxygen in $LaFeO_3$.

Diffuse reflectance spectra were recorded to investigate the optical characters of the samples. As shown in Figure 4a, compared to pristine LFO, P-LFO series samples present an obvious red-shift of the absorption edge to about 560 nm. It is because the acidification process may generate a highly protonated surface after calcination as well as the surface oxygen vacancies for light-harvesting.[26] The inset shows the $(\alpha h\nu)^{1/2}$ versus hν of LFO, P1-LFO, P2-LFO, and P3-LFO. The band gap values of the samples were determined to be around 2.0, 1.95, 1.92, and 1.91 eV, respectively. As indicated in Figure 3b, under light irradiation, the Nyquist plots of the P-LFO series presented much smaller semicircles in the high frequency region compared to that of pure $LaFeO_3$, indicating promoted charge separation and transport in photoexcited P-LFO series samples. With the increase of the phosphate modification, the semicircles of P2-LFO and P3-LFO were larger than that of P1-LFO, indicating that the proper treatment of phosphate was crucial to the transfer of electrons. The PL spectrum of P-LFO and $LaFeO_3$ with an excitation wavelength at 360 nm is shown in Figure S4. The PL emission intensities of the phosphate modified samples were weaker than that of the untreated sample, while the intensities of P2-LFO and P3-LFO were stronger than that of P1-LFO. The results from EIS and PL measurements indicate that the excess amount of phosphate used is unfavorable for charge transportation and separation.

Activation of N_2. The nitrogen activation ability of pure $LaFeO_3$ was also studied by the first principle. As shown in Figure S5, the optimized structural parameters of N_2 molecules were calculated by DFT according to the optimized structures. The extent of the N N triple bond weakening on the (121)

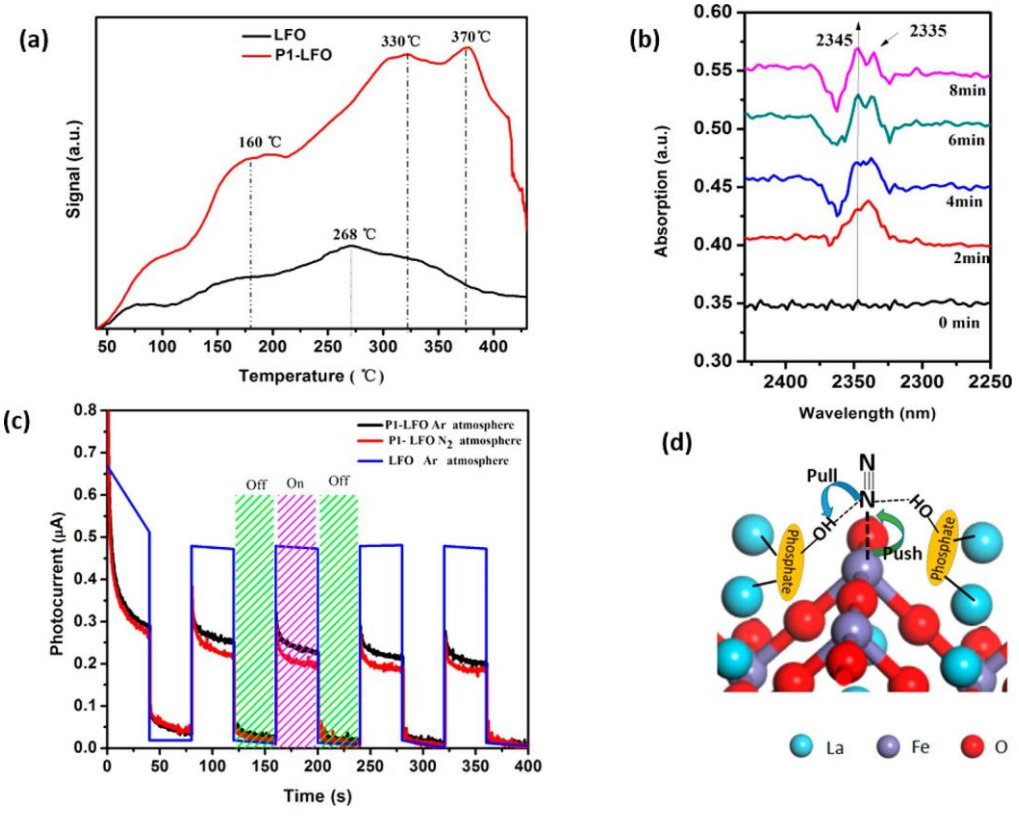

Figure 5. (a) N_2-TPD profiles of the as-prepared $LaFeO_3$ photocatalysts. (b) The in situ FTIR spectra recorded during the N_2 adsorption on P1-LFO. (c) The transient photocurrent of responses of different LFO photocatalysts in N_2 and Ar atmosphere. (d) Surface structure of phosphate modified LFO with the interaction of N_2.

facets of $LaFeO_3$ in this case can be observed visually by the N N triple bond increasing to 1.167 Å, which is between the free molecular N_2 (1.081 Å) and nitrene N_2H_4 (1.201 Å). As the chemical adsorption sites are regarded as active sites for N_2 activation, chemisorption is an essential step in N_2 photo-fixation. Temperature-programmed desorption (TPD) tests were conducted to evaluate the N_2 chemisorption on the surface of P-LFO and LFO. As indicated in Figure 5a, LFO presented two desorption peaks at 150 and 265 °C, attributed to the physical and chemical adsorption of N_2. For P1-LFO, the peaks ranging from 250 to 365 °C were related to the strong chemisorption of N_2. Notably, the peak of P1-LFO was more intense than that for pristine LFO, which is mainly attributed to the solid acid nature of modified phosphate groups. Generally, molecular N_2 with lone pair electrons presents Lewis base character, and is thus more easily chemisorbed by Lewis acid or the catalyst surface modified hydrogen bonding species. The TPD peak shifted to a higher temperature because of the delayed evolution of absorbed molecular N . The proposed

$_2$

surface modified groups Fe La O P OH stemming from the phosphate acid supported on LFO acted as Lewis acid sites and thus contributed to the enhanced N_2 adsorption and activation. Moreover, the additional peak of P1-LFO at 370 °C was also recorded, and additional N_2 adsorption sites of P1-LFO were detected. The indirect evidence of the enhancement of the N_2 adsorption and activation was shown in the in situ FTIR spectra (Figure 5b), and the peaks at 2334 and 2350 cm^{-1}, absent on pure LFO, are associated with the $\bar{\upsilon}$(N N) modes of N_2 adsorbed on the acidic sites.[27] The formation of OH−N_2 adducts as reported indicates the more efficient adsorption of N_2 on the catalyst surface under the atmosphere pressure.

In order to confirm the activation of the N_2, the photocurrent responses of the P1-LFO and LFO under N_2 and Ar atmosphere were also recorded as shown in Figure 5c. The photocurrent response reaches up to 0.46 μA for LFO and P1-LFO samples in Ar atmosphere. However, it is about 0.4 μA for LFO and 0.3 μA for P1-LFO in the N_2 saturated atmosphere, respectively. The decreased current response is mainly due to the interaction between the N_2 and catalyst. The transient photocurrent responses of both samples in N_2 saturated electrolyte were much smaller than that in the presence of Ar, indicating certain amounts of photoinduced electrons consumed by N_2. Noticeably, both the photocurrent curves of P1-LFO and LFO decreased at the beginning and then remained stable when the light was on, indicating that the electrons were captured by N_2 initially. Still, the photocurrent of P1-LFO was 25% lower than that of LFO, which contributed to the enhancement of N_2 adsorption and activation due to hydrogen bonding. Given the above discussion about N_2 dissociation on a phosphate modified surface, the electro-chemical measurements provide another convincing supple-ment to the TPD data for verifying the decisive role of phosphate within the LFO. Figure 5d shows a possible mechanism for improved N_2 activation via the synergistic effect of phosphate and transition metal Fe^{3+}, which is regarded as the “pull and push” strategy. In this model, the Fe^{3+} was suggested to be the first active site for N_2 activation, while the hydrogen bonds from phosphate modified on the La^{3+} sites were considered to be the additional N_2 active sites. Hydrogen bonding groups are commonly used in metalloenzymes to

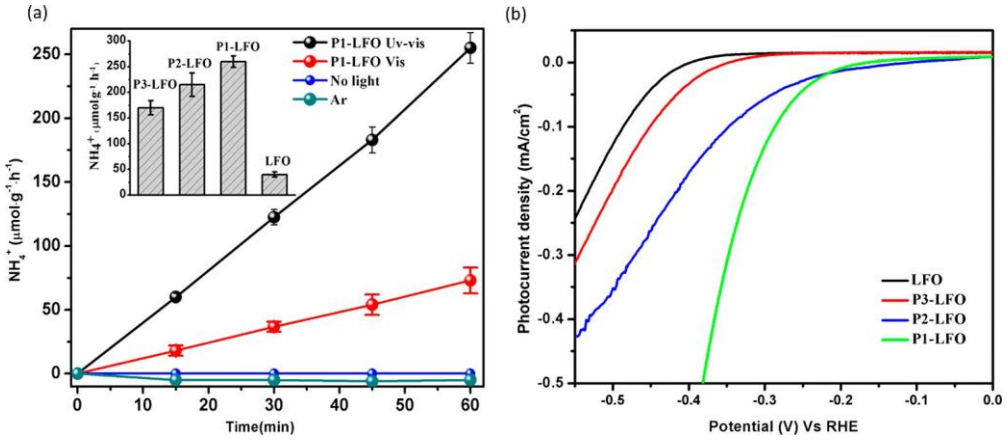

Figure 6. (a) Photocatalytic N_2 fixation rates of P1-LFO with time under UV−vis light (black), under visible light (red), in the dark (blue) in N_2 atmosphere, or under UV−vis light in Ar atmosphere (green), respectively. Inset: photocatalytic N_2 fixation rate of different samples. (b) The LSV curves of LFO and P-LFO series samples recorded in saturated N_2 electrolyte over time.

modulate substrate binding and activation, which lead to the polarization of N_2 to lower the activation barrier.

N_2 Photofixation Performance. On the basis of the theoretical prediction results, the N_2 photofixations over $LaFeO_3$ and various P-LFO samples were explored using water as the reactant in the absence of any organic scavengers or noble metal cocatalysts. Evidently, $LaFeO_3$ exhibited greatly enhanced N_2 photofixation reactivity after phosphate mod-ification. As shown in Figure 6, NH_3 production increased linearly, reaching 250 μmol g^{-1} h^{-1} after 60 min of irradiation over P1-LFO. The photocatalyst also exhibits good stability during the recycle test (Figure S6). The system did not evolve NH_3 in the absence of light irradiation or in an Ar atmosphere for comparison. As additional proof of N_2 photofixation, N_2H_4 was also detected in the form of an intermediate over $LaFeO_3$ and P1-LFO (shown in Figure S7). The N_2H_4 yields of P1-LFO and $LaFeO_3$ are only 10.3 and 1.45 μmol g^{-1} h^{-1}, while the NH_3 yields are dozens of times higher than those under full-spectrum irradiation, indicating the $LaFeO_3$-based photo-catalysts exhibit the excellent selectivity toward NH_3. The NH_3 production under visible light irradiation was 30% of that under UV−vis light. After 1 h of Xe lamp irradiation, only low NH_3 evolution (45 μmol g^{-1} h^{-1}) was detected over pure $LaFeO_3$. As shown in the inset to Figure 6, NH_3 evolution over P-LFO samples presented a monotonic increase with acid treatment, reaching about 250 μmol g^{-1} h^{-1} over P1-LFO, a 4.4-fold increase compared to pure LFO. With the excessive treatment of phosphate, however, the ammonia synthesis rates decreased mainly due to the block of electrons transferring. As indicated in the results of EIS, the phosphate modification also plays the important role in facilitating the H_2O dissociation and proton transfer. Linear sweep voltammetry (LSV) behavior of the proton transfer in the form of hydrogen evolution reaction (HER) over LFO and P-LFO series samples was examined in the N_2 saturated electrolyte under the Xe lamp irradiation. The overall potential of pure LFO was −0.5 V at 0.1 mA/cm^2 versus a reversible hydrogen electrode (RHE). When a moderate amount of phosphate was modified on the LFO surface, the overall potential of all the P-LFO samples exhibits positive shifts to −0.45, −0.40, and −0.38 V, respectively. The improved HER performance after phosphate mediation suggests that the phosphate is capable of effectively facilitating the H_2O dissociation and promoting the proton transfer on the LFO surface. This is concluded to be another reason for the improved N_2 photofixation performance, which is related to the protonation process of N_2. On the basis of the above analysis, the possible N_2 reduction on P-LFO is proposed as follows:

$$\text{P- LFO} + h\nu \rightarrow \text{P-LFO}(h^+ + e^-) \quad (1)$$

$$Fe^{3+} + e^- \rightarrow Fe^{2+} \quad (2)$$

$$Fe^{2+} + N_2 \rightarrow Fe^{3+} + N_2 \quad (3)$$

$$N_2 + 4e^- + 4H^+ \rightarrow N_2H_4 \quad (4)$$

$$N_2H_4 + 2e^- + 2H^+ \rightarrow 2NH_3 \quad (5)$$

$$6H_2O + 12h^+ \rightarrow 3O_2 + 12H^+ \quad (6)$$

First, simulated solar light excited electrons and holes are generated on the P-LFO catalyst (eq 1). Fe^{3+} species are reduced to Fe^{2+} by the photogenerated electrons (eq 2). The Fe^{2+} ions serve as the N_2 activation centers and donate the electrons to N_2, which promote the formation of activated N_2 species (*N_2) (eq 3). The photogenerated electrons reduce the *N_2 further and produce an N_2H_4 intermediate (eq 4) due to the synergistic N_2 activation effect from phosphate and transition metal $Fe^{3+/2+}$. The amount of hydrazine (N_2H_4) in the final product was about 4%, indicating that the N_2H_4 will be easily reduced to ammonia as detected (eq 5).[28] Meanwhile, the H_2O oxidation is another half-reaction besides N_2 photofixation, which provides sufficient protons for ammonia synthesis (eq 6).

CONCLUSION

Our work provides an alternative N activation strategy that weaken the triple N N bonds under [2]light irradiation by taking the "pull and push" strategy of nitrogenase to the photocatalysis fields. The outstanding N_2 photofixation performance (250 μmol g^{-1} h^{-1}) was achieved over phosphate modified (P1-LFO) as the positive results of the photocatalyst designation. The excellent N_2 photofixation performance is contributed to the synergistic effect of hydrogen bonding from phosphate and transition metals of $LaFeO_3$, which enhances the adsorption and activation of N_2. In addition, phosphate modification might serve as a universal strategy for the designation of the photocatalysts with sustainable N_2 conversion performance.

ASSOCIATED CONTENT

*

FTIR spectrum of pure $LaFeO_3$, XPS spectra, PL spectra, theoretical prediction of N_2 activation on $LaFeO_3$ (121) surface, cycle performance of N_2 photofixation over P1-LFO, and formation of N_2H_4 with P1-LFO and $LaFeO_3$ under full-spectrum irradiation of Xe lamp for 1 h (PDF)

AUTHOR INFORMATION

Corresponding Author

*E-mail: wzwang@mail.sic.ac.cn.

ORCID

Wenzhong Wang: 0000-0001-5983-3937

Author Contributions

§X.S. and D.J. are both first authors.

Notes

The authors declare no competing financial interest.

ACKNOWLEDGMENTS

This work was financially supported by the National Natural Science Foundation of China (51772312, 21671197, 51472260) and the research grant (16ZR1440800) from the Shanghai Science and Technology Commission.

REFERENCES

(1) Chalkley, M. J.; Del Castillo, T. J.; Matson, B. D.; Roddy, J. P.; Peters, J. C. Catalytic N_2 to NH_3 Conversion by Fe at Lower Driving Force: A Proposed Role for Metallocene-Mediated PCET. ACS Cent. Sci. 2017, 3 (3), 217−223.

(2) Zhu, D.; Zhang, L.; Ruther, R. E.; Hamers, R. J. Photo-illuminated diamond as a solid-state source of solvated electrons in water for nitrogen reduction. Nat. Mater. 2013, 12 (9), 836−841.

(3) Azofra, L. M.; Sun, C.; Cavallo, L.; MacFarlane, D. R. Feasibility of N_2 Binding and Reduction to Ammonia on Fe-Deposited MoS_2 2D Sheets: A DFT Study. Chem. - Eur. J. 2017, 23 (34), 8275−8279.

(4) Duman, L. M.; Farrell, W. S.; Zavalij, P. Y.; Sita, L. R. Steric Switching from Photochemical to Thermal Reaction Pathways for Enhanced Efficiency in Metal-Mediated Nitrogen Fixation. J. Am. Chem. Soc. 2016, 138 (45), 14856−14859.

(5) Sun, S.; An, Q.; Wang, W.; Zhang, L.; Liu, J.; Goddard Iii, W. A. Efficient photocatalytic reduction of dinitrogen to ammonia on bismuth monoxide quantum dots. J. Mater. Chem. A 2017, 5 (1), 201−209.

(6) Anderson, J. S.; Cutsail, G. E., 3rd; Rittle, J.; Connor, B. A.; Gunderson, W. A.; Zhang, L.; Hoffman, B. M.; Peters, J. C. Characterization of an Fe identical with N-NH_2 Intermediate Relevant to Catalytic N_2 Reduction to NH_3. J. Am. Chem. Soc. 2015, 137 (24), 7803−7809.

(7) Dong, G.; Ho, W.; Wang, C. Selective photocatalytic N_2 fixation dependent on g-C_3N_4 induced by nitrogen vacancies. J. Mater. Chem. A 2015, 3 (46), 23435−23441.

(8) Li, H.; Shang, J.; Ai, Z.; Zhang, L. Efficient Visible Light Nitrogen Fixation with BiOBr Nanosheets of Oxygen Vacancies on the Exposed {001} Facets. J. Am. Chem. Soc. 2015, 137 (19), 6393−6399.

(9) Yang, F.; Liu, C.; Gao, F.; Su, M.; Wu, X.; Zheng, L.; Hong, F.; Yang, P. The improvement of spinach growth by nano-anatase TiO_2 treatment is related to nitrogen photoreduction. Biol. Trace Elem. Res. 2007, 119 (1), 77−88.

(10) Hoffman, B. M.; Lukoyanov, D.; Yang, Z.-Y.; Dean, D. R.; Seefeldt, L. C. Mechanism of Nitrogen Fixation by Nitrogenase: The Next Stage. Chem. Rev. 2014, 114 (8), 4041−4062.

(11) Jia, H.-P.; Quadrelli, E. A. Mechanistic aspects of dinitrogen cleavage and hydrogenation to produce ammonia in catalysis and organometallic chemistry: relevance of metal hydride bonds and dihydrogen. Chem. Soc. Rev. 2014, 43 (2), 547−564.

(12) Hu, S.; Chen, X.; Li, Q.; Li, F.; Fan, Z.; Wang, H.; Wang, Y.; Zheng, B.; Wu, G. Fe^{3+} doping promoted N_2 photofixation ability of honeycombed graphitic carbon nitride: The experimental and density functional theory simulation analysis. Appl. Catal., B 2017, 201, 58−69.

(13) Zhao, W.; Zhang, J.; Zhu, X.; Zhang, M.; Tang, J.; Tan, M.; Wang, Y. Enhanced nitrogen photofixation on Fe-doped TiO_2 with highly exposed (101) facets in the presence of ethanol as scavenger. Appl. Catal., B 2014, 144, 468−477.

(14) Yoon, J. W.; Chang, H.; Lee, S. J.; Hwang, Y. K.; Hong, D. Y.; Lee, S. K.; Lee, J. S.; Jang, S.; Yoon, T. U.; Kwac, K.; Jung, Y.; Pillai, R. S.; Faucher, F.; Vimont, A.; Daturi, M.; Ferey, G.; Serre, C.; Maurin, G.; Bae, Y. S.; Chang, J. S. Selective nitrogen capture by porous hybrid materials containing accessible transition metal ion sites. Nat. Mater. 2017, 16, 526−531.

(15) Spatzal, T.; Perez, K. A.; Einsle, O.; Howard, J. B.; Rees, D. C. Ligand binding to the FeMo-cofactor: Structures of CO-bound and reactivated nitrogenase. Science 2014, 345 (6204), 1620−1623.

(16) Dance, I. The controlled relay of multiple protons required at the active site of nitrogenase. Dalton Trans. 2012, 41 (25), 7647−59.

(17) Liu, H. Z.; Li, X. N.; Hu, Z. N.; Cen, Y. Q.; Fu, G. P. Preparation chemistry of $Fe_{1-x}O$ based catalyst for ammonia synthesis. Chem. J. Chin. Univ. 2002, 23 (1), 87−91.

(18) Hoffman, B. M.; Dean, D. R.; Seefeldt, L. C. Climbing Nitrogenase: Toward a Mechanism of Enzymatic Nitrogen Fixation. Acc. Chem. Res. 2009, 42 (5), 609−619.

(19) Geri, J. B.; Shanahan, J. P.; Szymczak, N. K. Testing the Push-Pull Hypothesis: Lewis Acid Augmented N2 Activation at Iron. J. Am. Chem. Soc. 2017, 139 (16), 5952−5956.

(20) Liu, G.; Wang, T.; Zhang, H.; Meng, X.; Hao, D.; Chang, K.; Li, P.; Kako, T.; Ye, J. Nature-Inspired Environmental "Phosphorylation" Boosts Photocatalytic H_2 Production over Carbon Nitride Nanosheets under Visible-Light Irradiation. Angew. Chem., Int. Ed. 2015, 54 (46), 13561−13565.

(21) Hao, X.; Zhang, Y. Low temperature gel-combustion synthesis of porous nanostructure $LaFeO_3$ with enhanced visible-light photo-catalytic activity in reduction of Cr(VI). Mater. Lett. 2017, 197, 120− 122.

(22) Komova, O. V.; Simagina, V. I.; Mukha, S. A.; Netskina, O. V.; Odegova, G. V.; Bulavchenko, O. A.; Ishchenko, A. V.; Pochtar, A. A. A modified glycine−nitrate combustion method for one-step synthesis of $LaFeO_3$. Adv. Powder Technol. 2016, 27 (2), 496−503.

(23) Al-Omair, M. A.; Touny, A. H.; Saleh, M. M. Reflux-based synthesis and electrocatalytic characteristics of nickel phosphate nanoparticles. J. Power Sources 2017, 342, 1032−1039.

(24) Gabal, M. A.; Ata-Allah, S. S.; Al-Youbi, A. O.; Basahel, S. N.; Al-Thabaiti, S. A. Formation of $LaFeO_3$ and thermal decomposition reactions in lanthanum(III) oxalate−iron(II) oxalate crystalline mixture. J. Mater. Sci. 2006, 41 (22), 7597−7603.

(25) Li, Y.; Bian, Y.; Qin, H.; Zhang, Y.; Bian, Z. Photocatalytic reduction behavior of hexavalent chromium on hydroxyl modified titanium dioxide. Appl. Catal., B 2017, 206, 293−299.

(26) Chen, S.; Yan, R.; Zhang, X.; Hu, K.; Li, Z.; Humayun, M.; Qu, Y.; Jing, L. Photogenerated electron modulation to dominantly induce efficient 2,4-dichlorophenol degradation on BiOBr nanoplates with different phosphate modification. Appl. Catal., B 2017, 209, 320−328.

(27) Yoon, J. W.; Chang, H.; Lee, S. J.; Hwang, Y. K.; Hong, D. Y.; Lee, S. K.; Lee, J. S.; Jang, S.; Yoon, T. U.; Kwac, K.; Jung, Y.; Pillai, R. S.; Faucher, F.; Vimont, A.; Daturi, M.; Ferey, G.; Serre, C.; Maurin, G.; Bae, Y. S.; Chang, J. S. Selective nitrogen capture by porous hybrid materials containing accessible transition metal ion sites. Nat. Mater. 2017, 16 (5), 526−531.

(28) Chang, Y. H.; Chan, P. M.; Tsai, Y. F.; Lee, G. H.; Hsu, H. F. Catalytic reduction of hydrazine to ammonia by a mononuclear iron(II) complex on a tris(thiolato)phosphine platform. Inorg. Chem. 2014, 53 (2), 664−666.